ISSN 0016-7932, Geomagnetism and Aeronomy, 2023, Vol. 63, No. 7, pp. 925–936. © Pleiades Publishing, Ltd., 2023.

The Relationships between Cyclic Variations of Solar Magnetic Fields of Various Scales in Cycles 21–25

I. A. Bilenko*

Sternberg Astronomical Institute, Moscow State University, Moscow, 119234 Russia

**e-mail: bilenko@sai.msu.ru*

Received February 24, 2023; revised March 30, 2023; accepted April 28, 2023

Abstract—In this paper, we present the results of a study of cyclic variations in magnetic fields of various scales in cycles 21–25: large-scale magnetic fields reflecting the dynamics of the global magnetic field of the Sun, the number of spots, which characterizes the dynamics of local magnetic fields of spots, and the intensity of radio emissions at a wavelength of 10.7 cm, which reflect variations in the magnetic fields of active regions and faculaes. The results showed that the general cycle changes in local fields and the corresponding oscillation spectra differs from those in the large-scale magnetic field. The dynamic correlation dependences show that the correlation between local and large-scale magnetic fields changes, both in each cycle, and from cycle to cycle. The correlation is at its minimum near the maximum and minimum phases of the solar activity. The correlation has an oscillatory character in the phases of growth and decline. The absence of clearly defined maxima in the general wavelet power spectrum of oscillations with periods from 82 days to 5 years is shown to be explained by the fact that the total spectrum is blurred over large time intervals due to the shift in the region of maximum intensity of individual periods, as well as a change in the width of the maximum intensity range from one Carrington rotation to another.

DOI: 10.1134/S0016793223070058

1. INTRODUCTION

Solar magnetic fields differ both in their scale and in the nature of their behavior in the cycles of solar activity. Local magnetic fields have the maximum magnetic field strengths and their dynamics determines many flare and eruptive processes. Large-scale magnetic fields determine the dynamics of coronal holes and affect eruptive processes (Bumba and Obridko, 1969; Fainstein and Ivanov, 2010). The global magnetic field (GMF) of the Sun forms the structure and determines the parameters of the interplanetary magnetic field (Hoeksema, 1991; Zherebtsov et al., 1997). Magnetic fields of all scales contribute to the state of space weather in the Earth's orbit.

The regularities of the formation, cyclic evolution, and interdependence of magnetic fields of different scales are incompletely understood.

According to Leighton's theory (Leighton, 1964; 1969), the GMF of the Sun is a decay product of local magnetic fields of active regions (ARs). However, the GMF dynamics was shown in (Makarov et al., 1989a, b) not to depend on ARs; the GMF precedes ARs by approximately 5.5 years. The study of the dependences between the GMF and ARs (Bilenko, 2016) showed that the interdependencies between the GMF and AR parameters are different, both in general in different cycles and in different phases in different cycles, which may indicate different sources of the magnetic fields formation of ARs and the GMF. The dynamics of background magnetic fields, which are one of the manifestations of the GMF, also differs from the dynamics of strong AR magnetic fields (Bilenko, 2020a).

Over the past four cycles, there was a decrease in GMF (Wang et al., 2009; Bilenko, 2018). However, the magnetic fields of sunspots, i.e., local magnetic fields, do not reveal a long-term trend to decreasing magnetic fields (Pevtsov et al., 2011), which may indicate that local magnetic fields are not the cause of the observed decrease in the total magnetic field of the Sun.

The dynamics of magnetic fields of different scales differs in different cycles. The anomalous behavior of global and large-scale magnetic fields in cycle 23 was noted in (Obridko and Shelting, 2009).

This study was aimed at comparing the cyclic variations of local and large-scale magnetic fields of the Sun based on WSO observations of solar photospheric large-scale magnetic fields that reflect the dynamics of the solar GMF, changes in the number of spots characterizing the behavior of local magnetic fields of spots, and the intensity of radio emissions at a wavelength of 10.7 cm, which reflect the dynamics of local magnetic fields of active regions and faculaes.

2. DATA

The period of cycles 21–24 and the beginning of cycle 25 (1976–2022 or 1642–2258 Carrington rotations or CRs) is considered. Wolf numbers obtained from the SILSO (Sunspot Index and Long-term Solar Observations) database, the world data center for the creation, storage, and dissemination of international sunspot numbers, were used as an index of local magnetic field activity. The Greenwich catalog, which contains uniform data over a long period of time on the areas of sunspots, which are the best indicators of local magnetic fields, ends in 2016; this makes it impossible to take the 24th and the beginning of 25th cycle into account, thus the Wolf numbers were used. The study of Nagovitsyn, Pevtsov, and Osipova (Nagovitsyn, Pevtsov and Osipova, 2017) showed that the correlation between the magnetic field strength and the sunspot area varies depending on the phase of the solar cycle and that there are two populations of sunspots: those with a small area with weak magnetic fields and large spots with strong magnetic fields. Here, we studied the general ratios of magnetic fields of different scales and did not consider the possible differences when comparing a large-scale magnetic field and radio emission at a wavelength of 10.7 cm with spots of small and large areas. The Wolf numbers averaged over CR were used in the study. Wolf numbers are a synthetic index, but they provide information about the change in cycles of solar activity of the strongest magnetic fields: sunspot fields. The use of direct daily or high-resolution synoptic data of local photospheric magnetic fields compiled on their basis is not possible since there are no similar homogeneous data for the entire considered period. As well, the joint use of data from different ground-based and space observatories is difficult and does not give reliable unambiguous results throughout the required period (Virtanen and Mursula, 2016, 2017).

The intensity of radio emission at a wavelength of 10.7 cm ($F_{10.7}$) is used as a characteristic of local magnetic fields, but already includes the magnetic fields of all areas of ARs and photospheric faculaes. It was established using high-precision radio measurements that an increase in the intensity of radio emission is observed 1–2 days before the onset of AR formation and continues to be observed for another 1–2 days after the disappearance of ARs (Covington and Harvey, 1960). The values of the $F_{10.7}$ intensity of radio emission are measured in solar flux units (s.f.u); 1 s.f.u = 10^{-22} W m^{-2} s.

To analyze the cyclic dynamics of large-scale and GMFs of the Sun, observations of the WSO (Wilcox Solar Observatory) were used. We used synoptic data of a nonpolar magnetic field obtained from observations of large-scale photospheric magnetic fields for each CR, as well as the calculated coefficients of decomposition of the magnetic field into spherical harmonics.

3. COMPARISON OF CYCLIC VARIATIONS OF LOCAL AND LARGE-SCALE MAGNETIC FIELDS OF THE SUN

Figure 1 shows the cyclic changes in the Wolf numbers (W, Fig. 1a) averaged for each CR, which characterize variations in the strong local magnetic fields of spots, the intensity of radio emission at a wavelength of 10.7 cm ($F_{10.7}$, Fig. 1b), corresponding to the dynamics of ARs and faculaes and large-scale photospheric magnetic fields of positive ($Bp+$) and negative ($Bp-$) polarity and the sum of their modules (Bp, Fig. 1c). All parameters under consideration demonstrate a decrease in both the maximum and minimum values from 21 to 24 cycle (Bilenko, 2018). The values of all parameters at the initial growth phase of the 25th cycle are higher than those for the corresponding period of the 24th cycle, but lower than those in the high 21st and 22nd cycles.

Figure 2 shows the combined graphs of cyclic variations smoothed over 7 CRs averaged over each CR for W (thin line), $F_{10.7}$ (thick line), and Bp (dashed line) normalized to their maximum values. It follows from Fig. 2 that in all cycles at the growth phases of solar activity, the growth of Bp precedes the growth of W, and at the phases of decline, the decrease in Bp lags behind W. A complete explanation of this relationship in the growth phase requires additional consideration. However, such behavior of Bp at the growth phase indicates an independent mechanism of the formation of a large-scale magnetic field. The delay of Bp from W at the decay phase may be due to the fact that during this period the local magnetic fields of AR decay make a large contribution to the large-scale magnetic field.

The $F_{10.7}$ radio emission significantly outpaces the growth of both W and Bp in the solar-activity growth phase and also lags behind them in the decay phase since it is formed before the appearance and continues to be observed after the disappearance of ARs (Covington and Harvey, 1960). In the low cycles 23 and 24, $F_{10.7}$ is ahead of Bp and W in the growth phase and lags behind Bp and W in the decline phases, which have the maximum values. Similarly, for cycles 23 and 24, the relative change in intensity $F_{10.7}$ from the minimum to maximum activity is smallest in comparison with W and Bp.

In general, W, $F_{10.7}$, and Bp show a general trend of increasing values during growth phases and decreasing during decay phases. They correlate quite well with each other. For the entire considered period, the correlation coefficient between Bp and W is 0.928, between Bp and $F_{10.7}$ it is 0.949, and between W and $F_{10.7}$ it is 0.980. However, at all very high values, the correlation between Bp and W, i.e., between the large-scale magnetic field and the local magnetic field of spots, is the lowest.

In (Bilenko, 2016), it was shown that the correlation coefficients between the number and areas of sun-

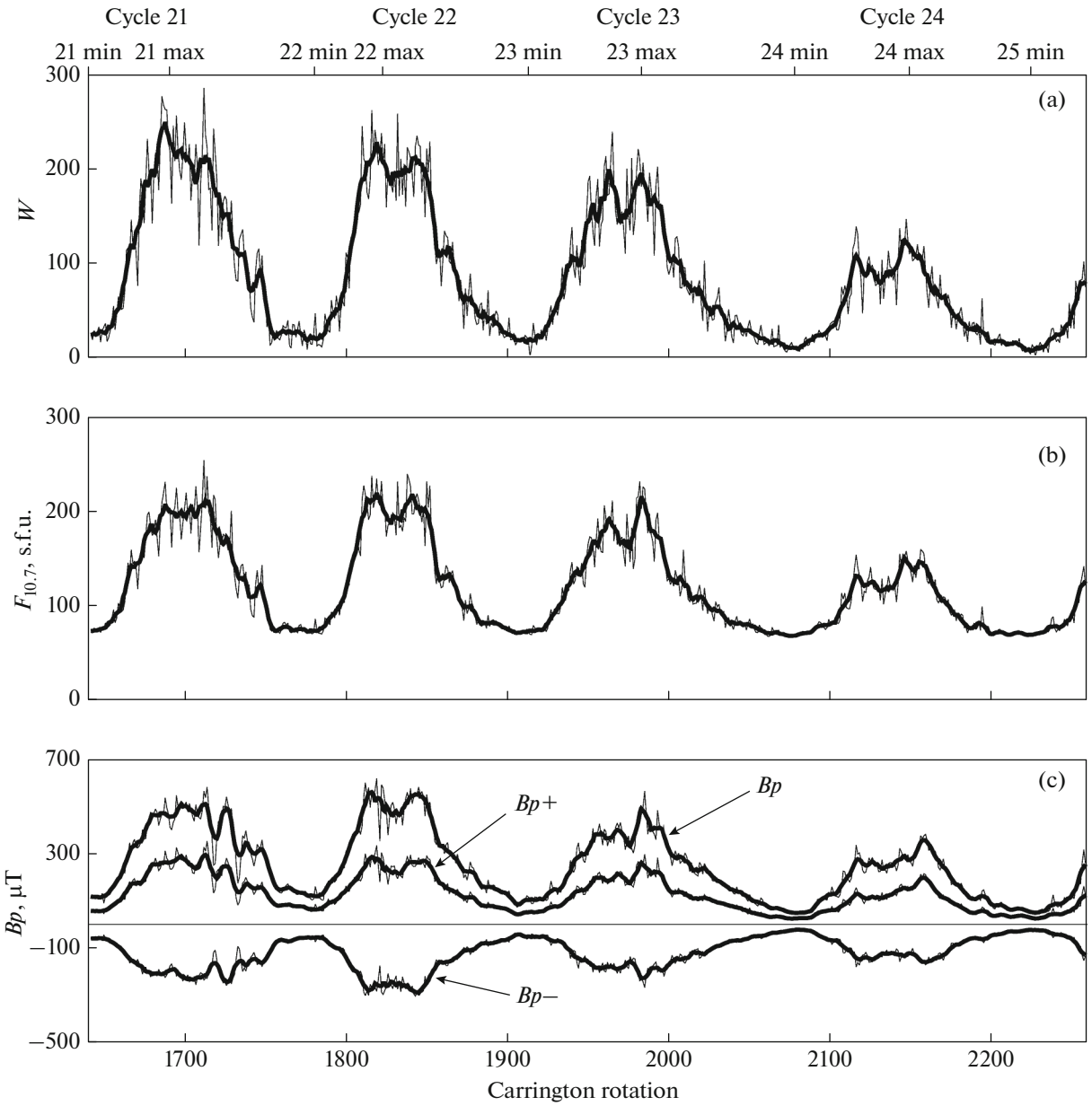

Fig. 1. The cyclic variations of average values: (a) Wolf numbers (*W*); (b) radiation at a wavelength of 10.7 cm; (c) the intensity of the non-polar large-scale photospheric solar magnetic field of positive (*Bp*+) and negative (*Bp*−) polarities and the sum of their modules (*Bp*) in cycles 21–25. The thin lines correspond to the average values for each CR, and the thick lines correspond to the values averaged over 7 CRs.

spots and GMF calculated at the source surface differ both from cycle to cycle and for the phases of growth, the maximum, and the decline of solar activity. Dynamic correlation dependences were built for a detailed consideration of the variations in the correlation coefficient between *W*, $F_{10.7}$, and *Bp* throughout the entire considered period (Fig. 3). For each pair of considered quantities, the correlation coefficients for seven CRs with a step of one CR were calculated. Then, the obtained values (thin lines) were smoothed over 15 CRs (thick lines) to identify characteristic trends. Based on the obtained correlation dependences, the correlation varies greatly and depends on the phase of the cycle. It is interesting to note that near the maxima and minima of all cycles, there is a significant decrease in the correlation coefficient for the $Bp-W$ and $Bp-F_{10.7}$ dependences. For the $W-F_{10.7}$ dependences, similar decreases in the correlation coefficient are also observed; they had the largest amplitude in cycle 24. In the phases of growth and decline, the correlation dependences are oscillatory.

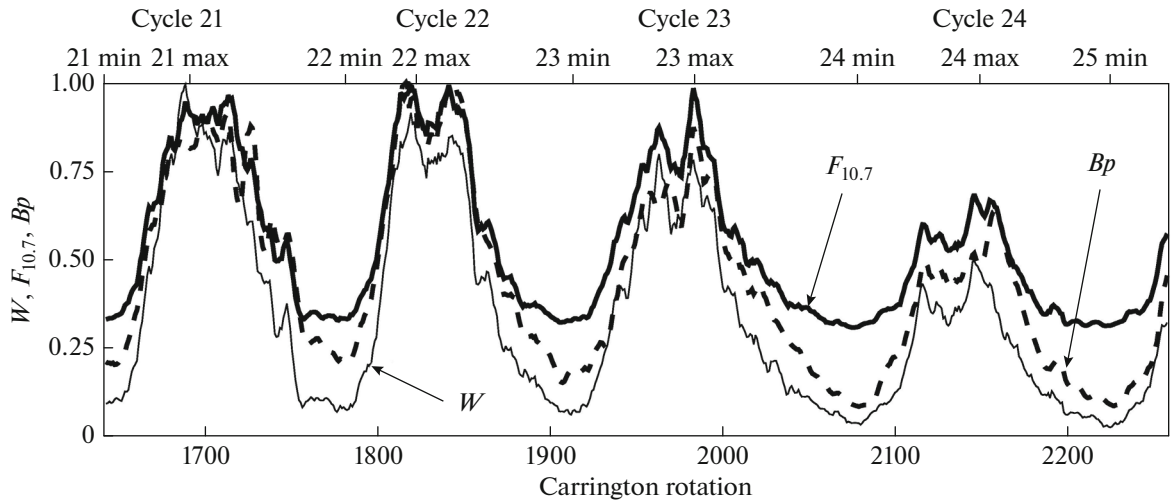

Fig. 2. The combined graph of the averages for each CR for W, $F_{10.7}$, and Bp, averaged over 7 CRs normalized to their maximum values.

4. WAVELET ANALYSIS OF W, $F_{10.7}$, AND Bp

Figure 4 shows the wavelet spectra of W (Fig. 1a), $F_{10.7}$ (Fig. 1b), and the total strength (the sum of the values of positive and the module of negative large-scale magnetic fields) Bp (Fig. 4c). The Morlet wavelet transform was used for the analysis. Oscillations with periods of 3–6 CRs (P1, 0.22–0.45 yr or 82–164 days), 6–17 CRs (P2, 0.45–1.27 yr or 164–64 days), 17–70 CRs (P3, 1.27–5.23 years or 464–1909 days), and 70–200 CRs (P4, 5–15 years), whose boundaries are marked on the spectra by horizontal lines, are distinguished in all spectra. At the general similarity of the dynamics of oscillations in the Bp, $F_{10.7}$, and W spectra in the cycles of solar activity, obvious differences are also visible. In the general power spectrum of Bp, there is no oscillation peak in the P1 range, which is observed in the W spectrum and weaklier in the $F_{10.7}$ spectrum. The ranges of increased intensity and their maximum values within periods P1–P4 differ both for different cycles and for W, $F_{10.7}$, and Bp. Figure 4 shows that the areas of increased intensity of oscillations of periods P1–P3 are constantly shifting each in its own range from one CR to another. As well, in each range, the intervals of periods P1–P3 corresponding to the maximum intensities of oscillations also change. This leads to the fact that the total value for each of the ranges of the P1–P3 periods does not have a single clearly defined maximum in the total oscillation power spectrum (right graphs) for cycles 21–25, but represents some average value blurred for each range period. While at shorter time intervals in each individual cycle, not only are maxima distinguished, a complex structure of changes in the intensity of these oscillations is also visible for example, for oscillations of the periods P1 and P2. This is the reason that the well-known 2-year oscillations corresponding to the P3 oscillation range are well distinguished in each individual cycle and at short time intervals (for example, at individual phases of the cycle), but are practically lost when averaged over large time scales.

The maximum values of the intensity of oscillations of the P4 range in cycles 21–22 occupy almost the entire range of periods from 70 to 200 CRs. However, in the 23rd, 24th, and early 25th cycles, the range of periods is narrower, which, despite a decrease in power in this epoch, leads to the fact that in the total power spectrum for cycles 21–25 the signal in the P4 period is less blurred than that in the P1–P3 periods.

Figure 5 shows the cyclic variations of the average values of the oscillation intensity for each range for periods P1–P4. Fluctuations are indicated by a thick line for the P1 range, by a thin line for P2, by a dashed line for P3, and by a dash-dotted line for P4. Since the average values were calculated for each range, their cyclic variations may differ from the cyclic changes of individual specific periods. For convenience in comparing the intensities of different ranges, the values of P3 and P4, and P2 for Bp were brought to a common scale. The intensity values are divided by 100 for P4, by 4 for P3, and by 2 for P2 for Bp. Figure 5 shows that fluctuations in the P1 and P2 ranges are observed during the phases of growth, the maximum, and the decline of solar activity and are absent during periods of minima. The maximum amplitudes of these fluctuations are observed at the maxima of solar activity. In this case, oscillations P1 of the local magnetic fields W and $F_{10.7}$ have the maximum amplitude in odd cycles and a minimum in even ones. In this case, the P1 amplitude in cycle 21 is higher than that in cycle 23, and in cycle 22, it is higher than that in cycle 24. This regularity is not observed for P1 oscillations in the Bp spectrum, where P1 oscillations have the maximum amplitude in cycle 22. The increase in the intensity of

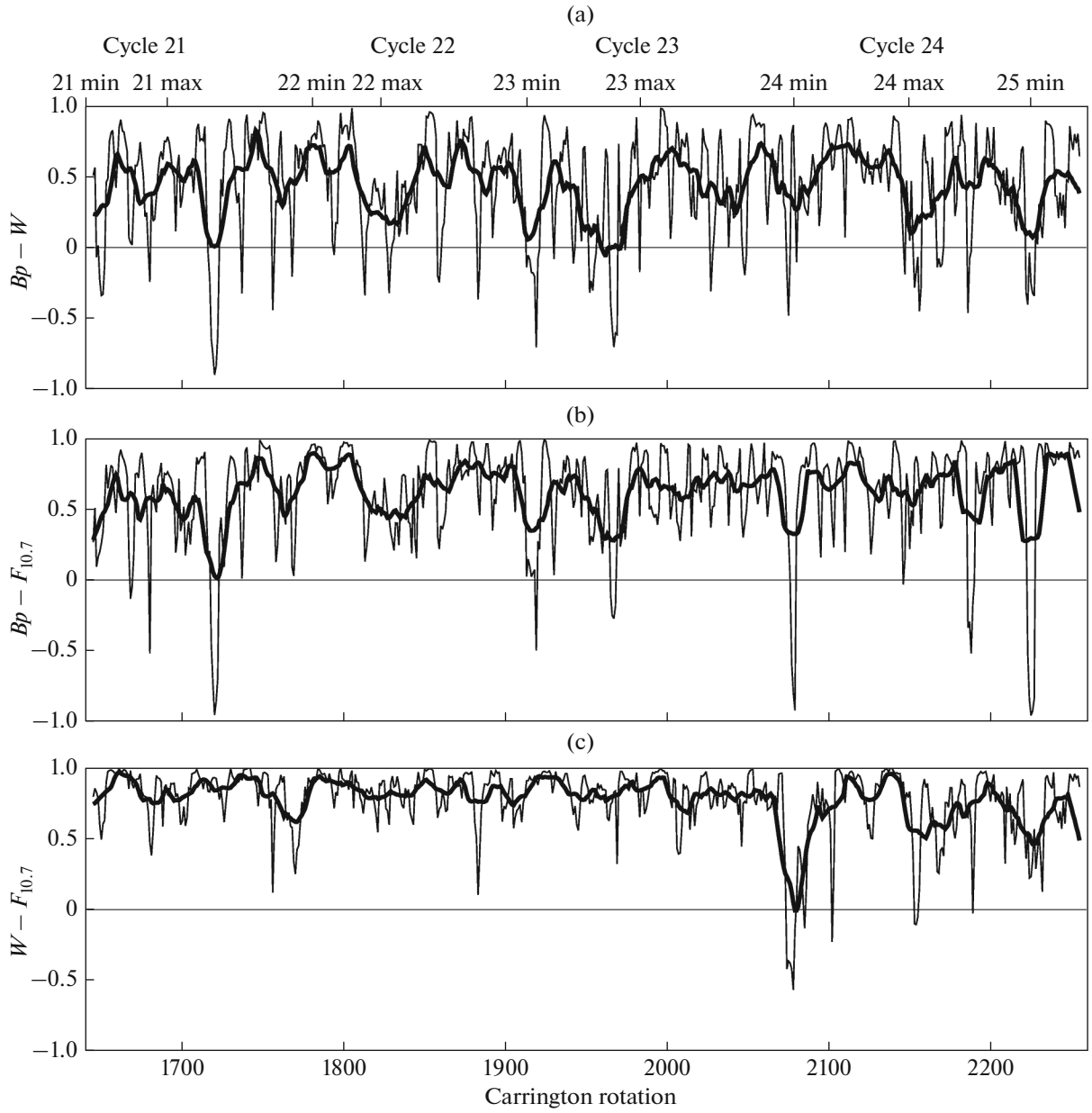

Fig. 3. The cyclic variations of the dynamic correlation coefficient between: (a) the strength modulus of a non-polar large-scale photospheric magnetic field and the Wolf numbers (Bp–W); (b) the intensity modulus of a non-polar large-scale photospheric magnetic field and radiation at a wavelength of 10.7 cm (Bp–$F_{10.7}$); Wolf numbers and radiation at a wavelength of 10.7 cm (W–$F_{10.7}$). Thin lines correspond to the values of the correlation coefficient calculated for every seven successive CRs with a step of 1 CR, and thick ones correspond to the obtained values averaged over 15 CRs.

fluctuations of P1 periods in cycle 25 is higher in the spectrum of Bp and it exceeds the values for the same period in cycles 23 and 24. The maximum values of P2 in the W spectrum have the highest values in cycle 21 while, in cycles 22–24, they remain approximately at the same level. In the $F_{10.7}$ spectrum, they are at a maximum in cycles 22 and 23 while in the Bp spectrum, they are at a maximum in cycle 21.

Variations in the intensity of oscillations in the P3 range partially coincide for W, $F_{10.7}$, and Bp. They are at a maximum at the maximums and at their minimum at the minimums of solar activity. However, the intensity of fluctuations in the P3 range of local magnetic fields of W and $F_{10.7}$ gradually decreases from cycle 21 to cycle 25, and in the Bp spectrum, the intensity of fluctuations P3 is approximately at the same level in cycles 21 and 22, sharply decreases to cycle 23, and then slightly increases in the cycle 24. Unlike the P1 and P2 fluctuations, the fluctuation intensity of P3 period does not decrease to zero at activity minima. In

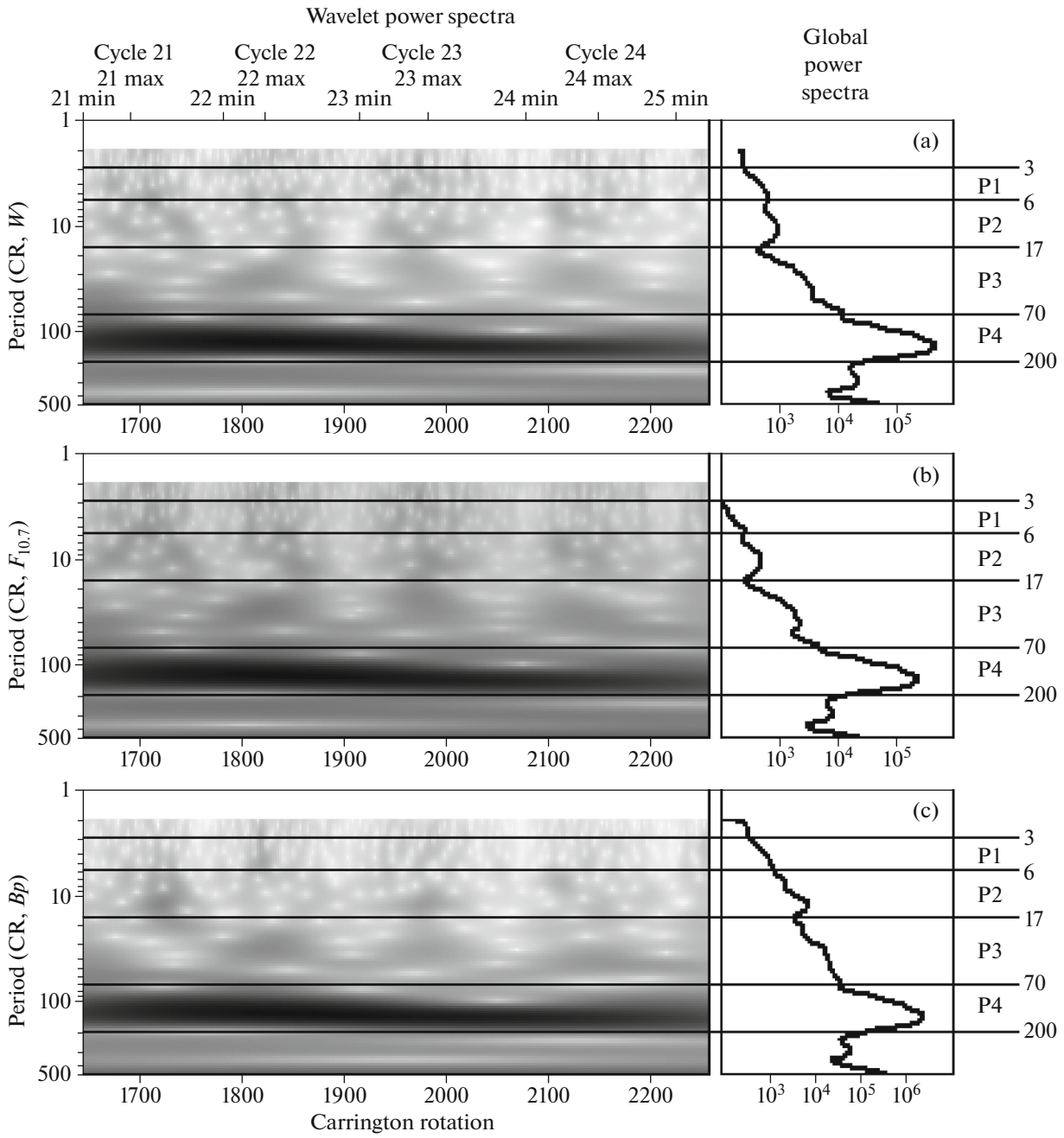

Fig. 4. The wavelet spectra of values averaged over CRs: (a) Wolf numbers (W); (b) radiation at a wavelength of 10.7 cm ($F_{10.7}$); (c) strength modulus of a non-polar large-scale photospheric magnetic field (Bp).

the cycle 25, the intensity of the P3 oscillations in the Bp spectrum is still at the level of cycle 23. The duration of the existence of fluctuations in the P1–P3 ranges is at its minimum in cycle 24.

The changes in the intensity of fluctuations in the P4 range practically coincide in time for W, $F_{10.7}$, and Bp. The intensity of P4 fluctuations increases from cycles 21 to 22, reaching a maximum at the growth phase of cycle 22 for both W, $F_{10.7}$ and Bp, and then gradually decreases, reaching almost a 5 times lower value at the beginning of cycle 25.

To compare the cyclic changes in fluctuations in the P1–P4 ranges, Fig. 6 shows the combined graphs of oscillations of the same frequency intervals for W (thin lines), $F_{10.7}$ (thick lines), and Bp (dashed lines) each normalized to its maximum value. Figure 6 shows that the nature of cyclic changes in oscillations with periods P1–P2 is similar in time for the spectra of local W and $F_{10.7}$ magnetic fields and differs significantly from the oscillations of the Bp spectrum. The Bp and $F_{10.7}$ P3 fluctuations are ahead of the W P3 fluctuations in the growth phases of cycles 22–25 and

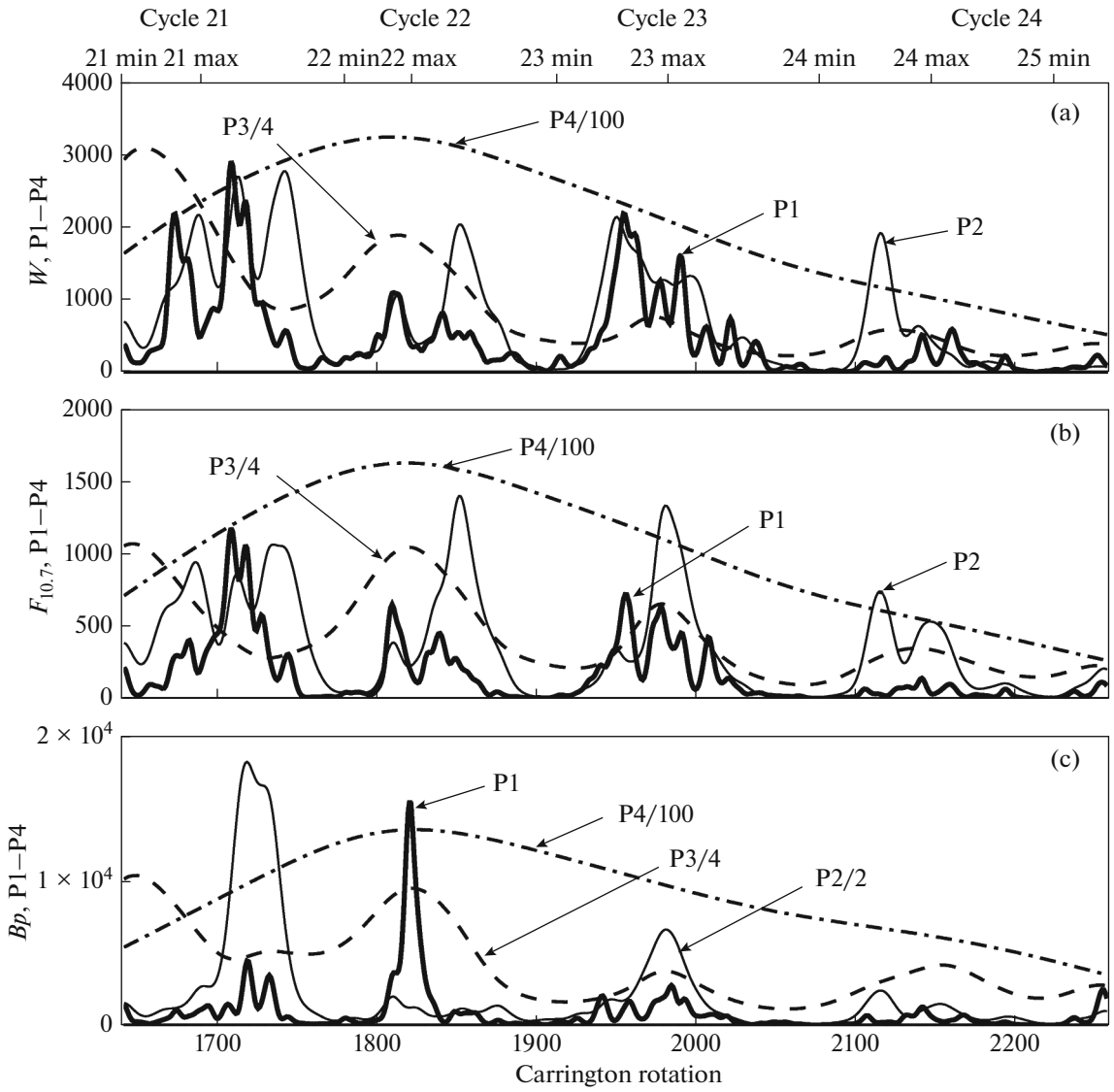

Fig. 5. The average oscillation intensities obtained from the wavelet spectra in the ranges of periods P1, P2, P3, and P4: (a) Wolf numbers (W); (b) radiation at a wavelength of 10.7 cm ($F_{10.7}$); (c) intensity modulus of a nonpolar large-scale photospheric magnetic field (Bp).

lag behind in the decline phases in cycles 22–24, which is consistent with the nature of the relationships between W, $F_{10.7}$, and Bp (Fig. 2). However, the fluctuations of the P3 periods for $F_{10.7}$ are ahead of the fluctuations of the P3 period for W and Bp in the decline phase of cycle 21 and are ahead of the fluctuations of the P3 period for Bp in the decline phase in cycle 24.

Figure 7 shows the cyclic variations of the ratios of the oscillation intensities with the ranges of periods P1–P4. For convenience, all dependences were reduced to a single scale. Figure 7 shows that the ratios of the oscillation intensities are different in different cycles, and they differ for W, $F_{10.7}$, and Bp. The ratio of fluctuations in the range P4 to P1 is at its maximum for Bp and reaches its maximum value in cycle 23, fluctuations in the range P4 to P3 are at their maximum in cycles 22 and 23 for all indices, P3 to P1 are higher in the low cycles 23 and 24, and P2 to P1 are higher in cycles 22 and 24 for W and $F_{10.7}$. It should be noted that the growth in the ratios with P1 and P2 at solar activity minima is largely caused by a sharp decrease in their values during these periods.

5. CYCLIC CHANGES OF HARMONICS IN SPHERICAL HARMONIC ANALYSIS OF THE GMF

The solar magnetic field can be described as a function of latitude and longitude coordinates (r, θ, φ) (Altschuler and Newkirk, 1969; Altschuler et al., 1975; Chapman and Bartels, 1940):

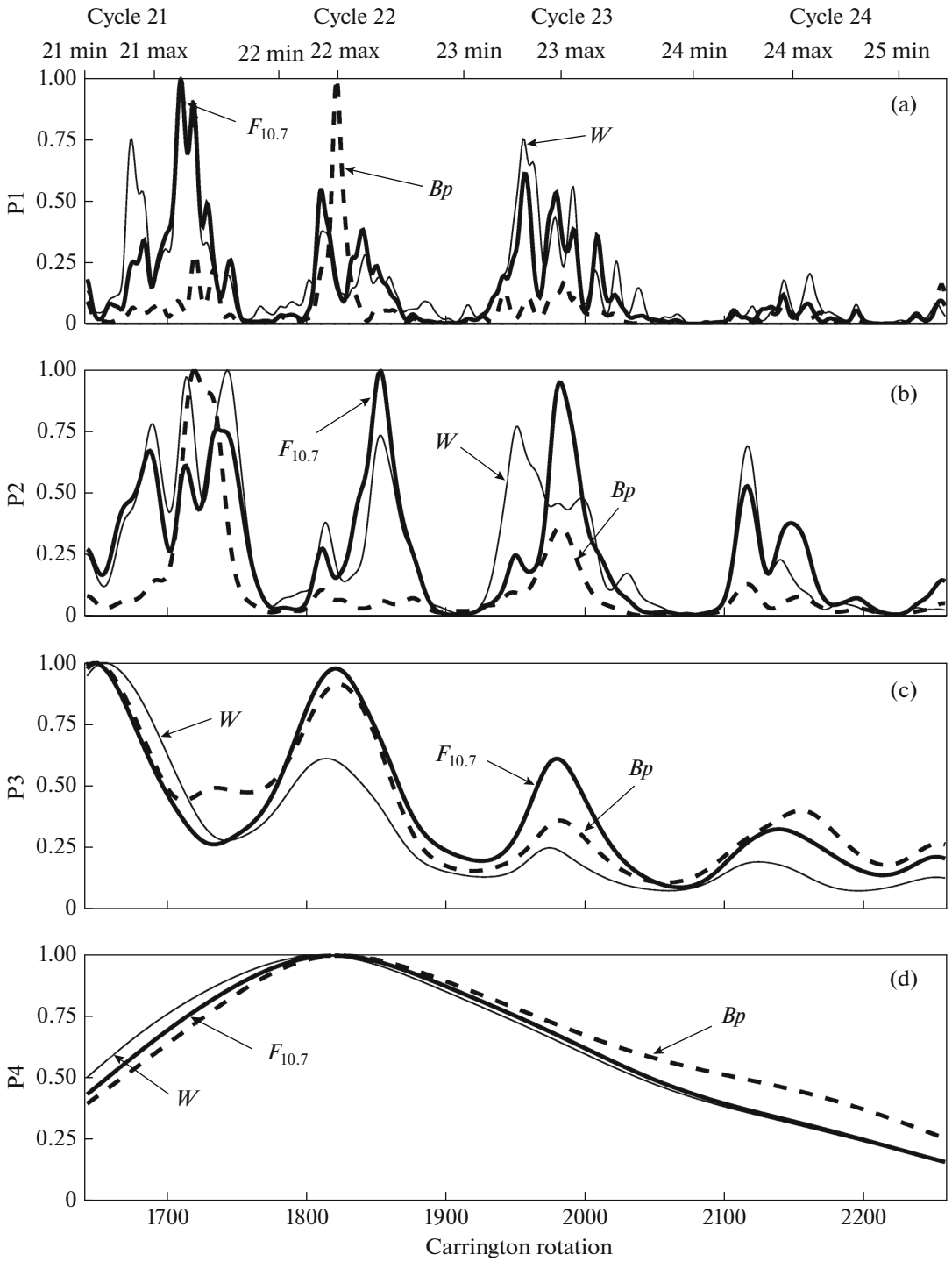

Fig. 6. The combined intensities of oscillations W, $F_{10.7}$, and Bp normalized to their maximum values in the ranges of periods: (a) P1; (b) P2; (c) P3; (d) P4.

$$\psi(r,\theta,\varphi) = R\sum_{n=1}^{N}\sum_{m=0}^{n}\left(\frac{R}{r}\right)^{n+1}$$
$$\times [g_n^m \cos(m\phi) + h_n^m \sin(m\phi)]P_n^m(\theta),$$

where $P_n^m(\theta)$ are the associated Legendre polynomials; N is the number of harmonics; and coefficients: g_n^m, h_n^m are calculated by fitting with the least squares method of the observed radial component of the photospheric magnetic field in the potential approximation. The formula describes the solar magnetic field as the sum of individual functions. Based on g_n^m, h_n^m coefficients, the power spectrum of various harmonic components can be obtained (Altschuler et al., 1977; Levine, 1977; Stix, 1977):

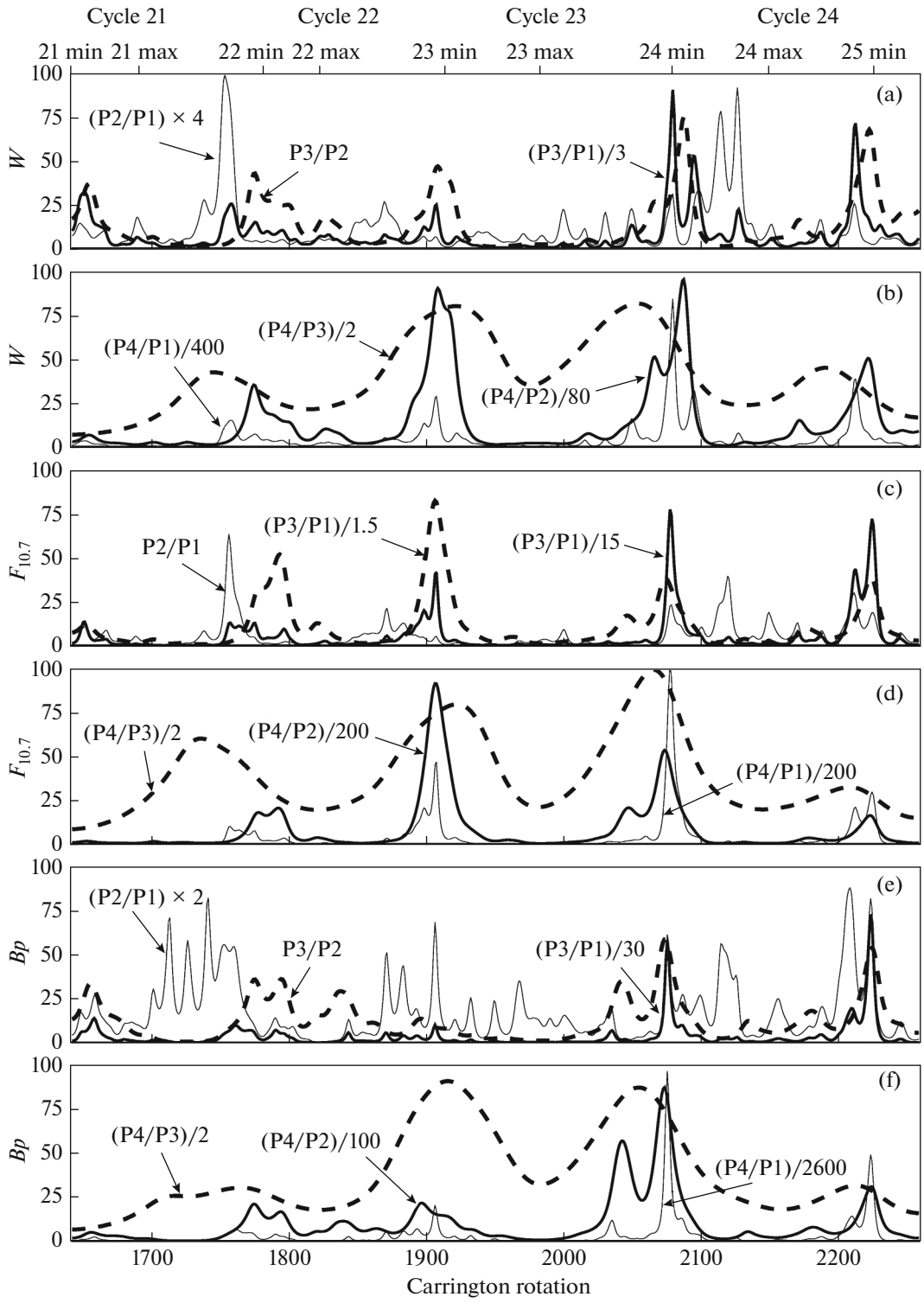

Fig. 7. The changes in the ratio of oscillation intensities in the ranges of periods P1–P4 in cycles 21–25.

$$S_n = \sum_{m=0}^{n} [(g_n^m)^2 + (h_n^m)^2].$$

Each harmonic, as defined by its indices (n, m), corresponds to the contribution of certain magnetic fields to the overall distribution. The purely latitudinal distribution of magnetic fields is described by harmonics with the index $m = 0$. Such functions are called zonal. When $n = m$, the functions are called sector. These are alternating meridional regions of magnetic fields of positive and negative polarity.

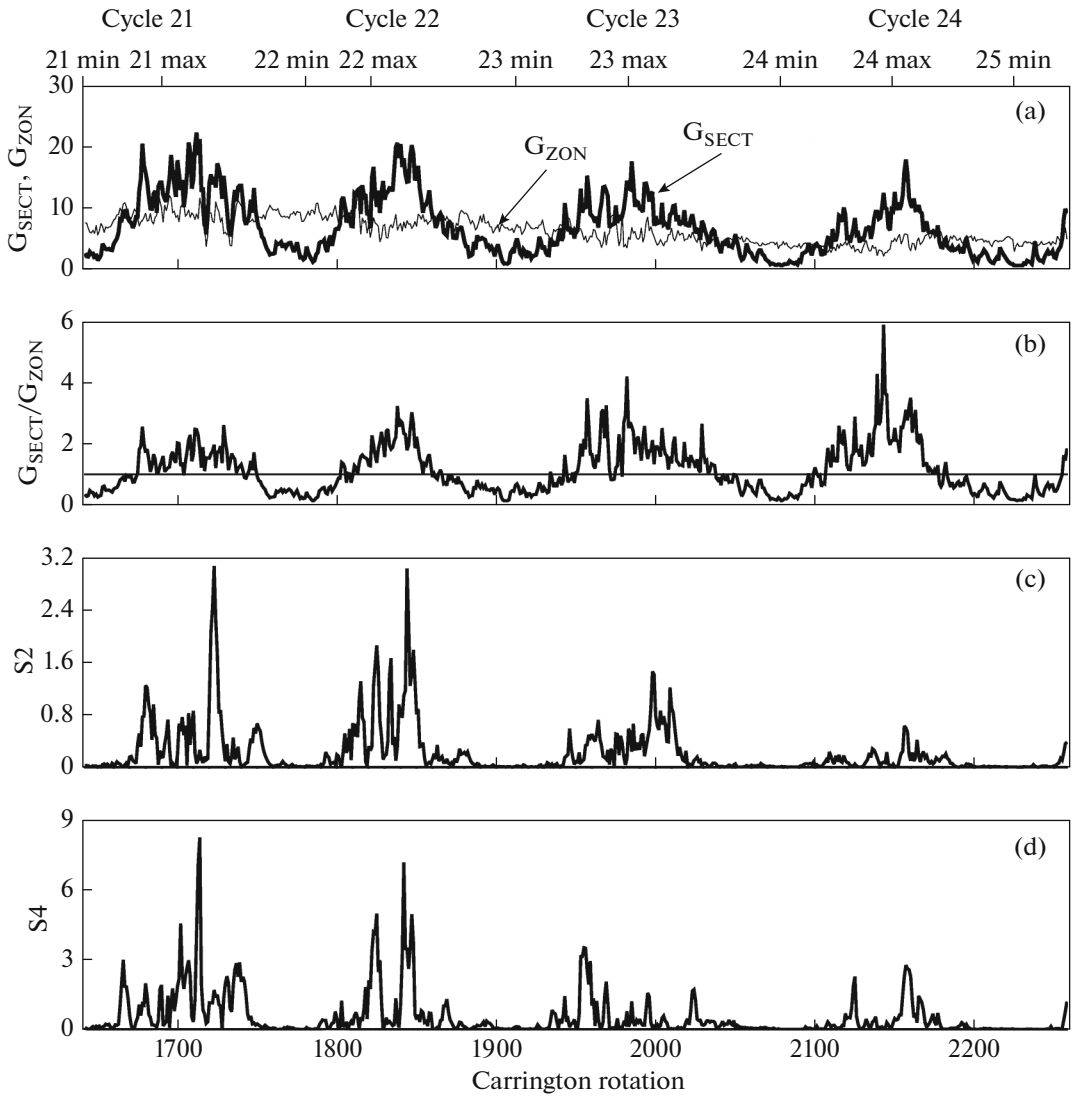

Fig. 8. The cyclic changes in the harmonics of the spherical harmonic decomposition of the global magnetic field of the Sun: (a) the sum of zonal harmonics (G_{ZON}, thin line) the sum of sectoral harmonics (G_{SECT}, thick line), (b) the ratio of the sum of sectoral to the sum of zonal components, (c) sector component S2, and (d) sector component S4.

Figure 8 shows the cyclic variations of the harmonics of the spherical harmonic analysis of solar GMF according to the WSO data. Figure 8a shows the changes in the sum of sector (G_{SECT}, thick line) and zonal (G_{ZON}, thin line) harmonics. The change in their ratio in the cycles of solar activity is shown in Fig. 8b. The cyclic evolution of GMF is characterized by a transition from the zonal structure of the distribution of magnetic fields, which is typical for solar activity minima, to the sector structure in the phases of growth, the dominance of the sector structure at the maximum activity, and the reverse transition from the dominance of the sector structure of the distribution of magnetic fields to the zonal structure in the late phases of decline solar activity. The variations of sector harmonics correspond to the general course of cyclic changes of W, $F_{10.7}$, and Bp and fluctuations of the P1–P3 periods.

Figure 8c shows the variations of the S2 sector harmonics ($n = m = 2$), and Fig. 8d shows the variations of the S4 sector harmonics ($n = m = 4$). When analyzing the global magnetic field (Bilenko, 2020b), it was shown that certain GMF structures correspond to oscillations of certain periods and their changes in the cycle correspond to variations in specific harmonics. Figure 8 shows that there is a decrease in the intensity of the sum of zonal harmonics from cycle 21 to cycle 25. The intensity of the sum of sector harmonics is approximately at the same level in cycles 21 and 22; it then slightly decreases to cycles 23 and 24. The maximum values are approximately the same in cycles 23 and 24. In this case, the relative contribution of sector

harmonics is higher in cycles 23 and 24. Cyclical changes in the maximum values of the S2 and S4 sector harmonics are more consistent with variations in the P3 range of the *Bp* spectrum, i.e., large-scale magnetic fields.

6. CONCLUSIONS

We presented the results of a study of cyclic variations in magnetic fields of various scales in cycles 21–25, that is, the large-scale magnetic fields (*Bp*) that reflect the dynamics of solar GMF, sunspot numbers (*W*) characterizing the dynamics of strong local magnetic fields of spots, and radio emission intensity at a wavelength of 10.7 cm that reflect variations of the magnetic fields of active regions and faculae.

For the entire considered period, the correlation coefficients are 0.980 between *W* and $F_{10.7}$, 0.949 between *Bp* and $F_{10.7}$, and the lowest, 0.928, between *Bp* and *W*. Near the maxima and minima of the cycles, a decrease in the correlation coefficient is observed. In the phases of growth and decline, the correlation dependences have an oscillatory character.

Comparison of cyclic variations of the indices of local (*W* and $F_{10.7}$) and large-scale (*Bp*) magnetic fields showed that the general course of cyclic changes in local fields differs from similar ones in a large-scale field. The precedence of *Bp* in the growth phases with respect to *W* indicates an independent mechanism for the formation of a large-scale magnetic field.

A detailed analysis of the *W*, $F_{10.7}$, and *Bp* wavelet spectra also showed that the ratios of the oscillation intensities of the wavelet spectra of the indices of local *W*, $F_{10.7}$ magnetic fields, and *Bp* large-scale magnetic field and their dynamics in cycles differ significantly both in the nature of changes in the ranges of periods P1–P3 and from cycle to cycle. The ranges of increased intensity and their maximum values in periods P1–P3 differ both for different cycles and for *W*, $F_{10.7}$, and *Bp*.

The absence of clearly defined maxima in the total power spectrum of fluctuations in periods P1–P3 (from 82 days to 5 years) in cycles 21–25, which includes well-known 2-year fluctuations, is explained by the fact that the areas of increased intensity values of these fluctuations each shift its range from one CR to another, as well as the width of the periods of maximum intensity also changes. This leads to blurring of the total intensity for each range at large time intervals. On shorter time intervals, at individual phases of the cycle or in each individual cycle, not only are maxima distinguished, but for periods P1 and P2 a complex structure of changes in the intensities of these oscillations is visible.

The maximum values of the intensity of oscillations of the P4 range in cycles 21–22 occupy almost the entire range of periods from 70 to 200 CRs, but in cycles 23, 24, and early 25, the range of periods is narrower, which, despite a decrease in power in this epoch, leads to the fact that the signal in the P4 period is less blurred in the total power spectrum in cycles 21–25 than that in periods P1–P3.

Cyclic changes in the sum of sector harmonics and the S2 and S4 sector harmonics are more consistent with variations in the P3 period of the *Bp* spectrum, i.e., large-scale magnetic fields.

ACKNOWLEDGMENTS

In the work, we use sunspot data provided by the SILSO world center of the Belgian Royal Observatory, Brussels. The values of the intensity of radio emission at a frequency of 10.7 cm were obtained from the data of the Dominion Radio Astrophysical Observatory, Pentington, Canada, through the World Data Center for Solar-Terrestrial Physics WDCB, Moscow. The values of the GMF and harmonic coefficients are obtained from the data of the WSO (Wilcox Solar Observatory) solar observatory through the site http://wso.stanford.edu, which were provided by Dr. J.T. Hoeksema.

FUNDING

This work was supported by ongoing institutional funding. No additional grants to carry out or direct thisparticular research were obtained.

CONFLICT OF INTEREST

The author declares that she has no conflicts of interest.

REFERENCES

Altschuler, M.D. and Newkirk G., Jr., Magnetic fields and the structure of the solar corona, *Sol. Phys.*, 1969, vol. 9, pp. 131–149.

Altschuler, M.D., Trotter, D.E., Newkirk, G., Jr., and Howard, R., Tabulation of the harmonic coefficients of the solar magnetic fields, *Sol. Phys.*, 1975, vol. 41, pp. 225–226.

Altschuler, M.D., Levine, R.H., Stix, M., and Harvey, J., High resolution mapping of the magnetic field of the solar corona, *Sol. Phys.*, 1977, vol. 51, pp. 345–375.

Bilenko, I.A., Comparison of changes in the global magnetic field and spot activity in cycles 21 to 24, *Geomagn. Aeron. (Engl. Transl.)*, 2016, vol. 56, no. 8, pp. 978–986.

Bilenko, I.A., Determination of the coronal and interplanetary magnetic field strength and radial profiles from large-scale photospheric magnetic fields, *Sol. Phys.*, 2018, vol. 293, no. 7, id 106.

Bilenko, I.A., Relations between coronal mass ejections and the photospheric magnetic field in cycles 23 and 24, *Astrophys. J.*, 2020a, vol. 889, no. 1, id 1.

Bilenko, I.A., Manifestation of Rossby waves in the global magnetic field of the Sun during cycles 21–24, *Astrophys. J. Lett.*, 2020b, vol. 897, p. L24.

Bumba, V. and Obridko, V.N., 'Bartels' active longitudes', sector boundaries and flare activity, *Sol. Phys.*, 1969a, vol. 6, pp. 104–110.

Chapman, S. and Bartels, J., *Geomagnetism*, vol. 2, Oxford: Oxford Univ. Press, 1940.

Covington, A.E. and Harvey, G.A., The visibility of the 10-cm radio-emissive region and its application in finding the 10-cm quiet Sun, *Astrophys. J.*, 1960, vol. 132, p. 435.

Fainshtein, V.G. and Ivanov, E.V., Relationship between CME parameters and large-scale structure of solar magnetic fields, *Sun Geosphere*, 2010, vol. 5, pp. 28–33.

Hoeksema, J.T., Large-scale solar and heliospheric magnetic fields, *Adv. Space Res.*, 1991, vol. 11, pp. 15–24.

Leighton, R.B., Transport of magnetic fields on the Sun, *Astrophys. J.*, 1964, vol. 140, pp. 1547–1562.

Leighton, R.B., A magneto-kinematic model of the solar cycle, *Astrophys. J.*, 1969, vol. 156, pp. 1–26.

Levine, R.H., Evolution of photospheric magnetic field patterns during SKYLAB, *Sol. Phys.*, 1977, vol. 54, pp. 327–341.

Makarov, V.I. and Sivaraman, K.R., Evolution of latitude zonal structure of the large-scale magnetic field in solar cycles, *Sol. Phys.*, 1989a, vol. 119, pp. 35–44.

Makarov, V.I. and Sivaraman, K.R., New results concerning the global solar cycle, *Sol. Phys.*, 1989b, vol. 123, pp. 367–380.

Mordvinov, A. V. and Plyushina, L. A., Coherent structures in the dynamics of the large-scale solar magnetic field, *Astron. Rep.*, 2001, vol. 45, pp. 652–658.

Nagovitsyn, Y.A., Pevtsov, A.A., and Osipova, A.A., Long-term variations in sunspot magnetic field-area relation, *Astron. Nachr.*, 2017, vol. 338, no. 1, pp. 26–34.

Obridko, V.N. and Shelting, B.D., Anomalies in the evolution of global and large-scale solar magnetic fields as the precursor of several upcoming low solar cycles, *Astron. Lett.*, 2009, vol. 35, pp. 247–252.

Pevtsov, A.A., Nagovitsyn, Y.A., Tlatov, A.G. and Rybak, A.L., Long-term trends in sunspot magnetic fields, *Astrophys. J. Lett.*, 2011, vol. 742, L36.

Stix, M., Coronal holes and the large-scale solar magnetic field, *Astron. Astrophys.*, 1977, vol. 59, pp. 73–78.

Virtanen, I. and Mursula, K., Photospheric and coronal magnetic fields in six magneto graphs. I. Consistent evolution of the bashful ballerina, *Astron. Astrophys.*, 2016, vol. 591, A78.

Virtanen, I. and Mursula, K., Photospheric and coronal magnetic fields in six magnetographs. II. Harmonic scaling of field intensities, *Astron. Astrophys.*, 2017, vol. 604, A7.

Wang, Y.-M., Robbrecht, E. and Sheely, N.R.Jr., On the weakening of the polar magnetic fields during solar cycle 23, *Astrophys. J.,* 2009, vol. 707, pp. 1372–1386.

Zherebtsov, G.A., Kovalenko, V.A., and Molodykh, S.I., Heliospheric characteristics during fast global variations of solar magnetic fields, *J. Geophys. Res.*, 1997, vol. 102, pp. 2137–2146.

Translated by A. Ivanov